Supplemental Information

K. S. N. Vikrant[†], William Chueh[*], and R. Edwin García[†]

May 23, 2018

[†]:School of Materials Engineering,
Purdue University
[*]: Department of Materials Science and Engineering,
Stanford University

1 Grain Boundary-Grain Model Setup Generalities

A two-grain, bicrystal $\mathrm{Gd}_y\mathrm{Ce}_{1-y}\mathrm{O}_{2-y/2}$, GCO, with a planar grain boundary was modeled by placing the interface at the origin of the laboratory reference system. The normal of the interface was arbitrarily set to point along the x-axis. The degree of order of the structure was set to the analytical solution $\eta = 1-(1-\eta_\circ)\exp[-||x||/\delta]$, in agreement with the classic phase field literature, *e.g.*, Kobayashi *et al.* [1], Warren *et al.* [2], and Tang *et al.* [3]. Because of the symmetry of the two-grain system, the horizontal displacement at the center of the grain boundary was set to be zero, while set to expand freely in the vertical direction. The right edge (the grain) concentrations $[\mathrm{V}_\mathrm{O}^{\cdot\cdot}]_\infty$ and $[\mathrm{Gd}'_\mathrm{Ce}]_\infty$ were set based on the amounts of dopant and bulk charge neutrality, enabling to specify the grain boundary fields by self-consistently solving Equation 6 (main text). Electrically, the right edge (the grain) was set to be electrically grounded, and the left edge was solved via Equation 6. Based on Equations 1 to 5 in the main text, the segregation energy is non-zero at the grain boundary core and asymptotically drop off to zero $\delta = 2$nm away from the interface. The experimental total chemical expansion, β_T, of GCO was determined by Zha, Xia and Meng [4]. The experimental, macroscopic value, $\beta_T = 0.00095$, was attributed to $[\mathrm{Gd}'_{\mathrm{Ce}}]$ defects, based on the sensitivity analysis below. The $[\mathrm{V}_{\mathrm{O}}^{\cdot\cdot}]$ contribution to chemical expansion was neglected.

Table 1: Summary of Symbols.

Definition	**Name**
f	Helmholtz free energy per unit volume
$[V_N^{Z_N}]$	Mole fraction of Nth chemical species
η	Crystallinity order parameter
Z_N	Ionic valence of Nth chemical species
ρ	Electric charge density
ϕ	Electrostatic potential
$\vec{D}$	Total polarization
$\vec{E}$	Electric field vector
ϵ_r	Relative dielectric constant
ϵ	Absolute permittivity
$\overset{\leftrightarrow}{\sigma}$	Mechanical stress tensor
ε_{ij}	ijth component of total strain tensor
$\overset{\leftrightarrow}{\varepsilon}_e$	Elastic strain tensor
$\overset{\leftrightarrow}{\beta}^{(m)}$	Vegard tensor of mth species
$\beta_{ij}^{(m)}$	ijth component of Vegard tensor of mth species
$\vec{u}$	Mechanical displacement

Table 1: Summary of Symbols.

Definition	**Name**
T	Absolute temperature
Ω	Volume of solid
$\phi_\circ$	Interfacial electrostatic potential
Ω_{ij}	Interaction parameter of ith and jth species
$f^{S}_{V_{\ddot{O}}} - f^{X}_{V_{\ddot{O}}}$	Segregation energy of oxygen vacancies
$f^{S}_{Gd'_{Ce}} - f^{X}_{Gd'_{Ce}}$	Segregation energy of gadolinium defects
Z_O	Oxygen vacancies ionic valence
Z_{Gd}	Gadolinium defects ionic valence
$\Omega_{Gd'_{Ce}V_{\ddot{O}}}$	Interaction parameter of Gd'_{Ce} and $V_{\ddot{O}}$
δ	Grain boundary thickness
$\nu_\circ$	Atomic volume of Ceria
$\eta_\circ$	Degree of disorder in the interface
F	Faraday's constant
k_b	Boltzmann constant
E	Elastic modulus
ν	Poisson's ratio
σ_h	Hydrostatic stress
κ	Total electrical conductivity
D_i°	Self-diffusion coefficient of ith species
$E_{a,i}$	Activation energy of ith species for migration
$\beta^{(O)}$	Vegard expansion constant of oxygen vacancies
$\beta^{(Gd)}$	Vegard expansion constant of gadolinium defects

Table 1: Summary of Symbols.

Definition	**Name**
β_T	Experimental total chemical expansion
$p(\eta)$	$\eta^3(6\eta^2 - 15\eta + 10)$, Interpolation function

2 Numerical Setup

Equation set 6 was solved across a 20×20 nm simulation domain, and discretized into a 200×200 finite element mesh. The electrochemical part of the partial differential equations was solved by using `FiPy` [5]. The relative tolerance for the convergence was set to 1×10^{-8}. The mechanical equilibrium equation was solved using `OOF2` [6]. The relative tolerance for the convergence was set to 1×10^{-6}. The solution from one numerical framework was used as trial solution in the other one, and both solutions were iterated until the both electrochemical and chemomechanical calculations simultaneously reached the target relative tolerance. Each calculation took on the order of two hours of wall time to complete.

3 Polycrystalline Conductivity Model

The macroscopic ionic conductivity of the GCO polycrystal was calculated by generalizing the model proposed by Guo [7]. The total charge conductivity of the polycrystalline ceramic corresponds to the sum of ohmic losses from each of the differential elements of material, each of them described by the Nernst-Einstein equation, $d\kappa = \frac{e^2 Z_i^2 [V_i^{Z_i}] D_i}{k_B T}$, where $D_i = D_i^{\circ}[V_i^{Z_i}] \exp(-\frac{E_{a,i}([V_i^{Z_i}](x))}{k_B T})$. In agreement with McKee [8], and later by Guo [7], Guo and Waser [9], as well as Grieshammer and coworkers [11], and Pornprasertsuk *et al.* [12]. Each infinitesimal contribution to charge conductivity across the grain and grain boundary through-thickness of the polycrystal embodies the contributions from the space charge layer (through the depleted and segregated species and point defects), as well as the structural defects in the vicinity of the grain boundary. Here, the effects of defect-defect, defect-solute, and solute-solute interactions are captured in the solute-dependent activation energy, and by solving Equation 6 of the main text. The total conductivity is thus:

$$\kappa = \frac{L}{\displaystyle\int_0^L \frac{dx}{\sum_{i=1}^{N} \frac{e^2 Z_i^2 [V_i^{Z_i}]^2 D_i^\circ}{k_B T} \exp(-\frac{E_{a,i}([V_i^{Z_i}](x))}{k_B T})}} \tag{1}$$

The self-diffusion coefficient, $D_i^\circ = 6.1 \times 10^{-11}$ m^2/s, and activation energy data, $E_{a,i} = 2.4525[\mathrm{V}_{\mathrm{O}}^{\cdot\cdot}]+0.7629$ eV, for oxygen vacancies in GCO was obtained from [10, 11]. Attached to the re-submission of this manuscript, we have submitted a data file with the original simulation of GCO (simulatedData.txt), including the single-crystal response, the polycrystalline response without stress effects, and the predicted polycrystalline conductivity data with stress effects. The experimental polycrystalline total conductivity was also posted. The data file is compatible in Windows, Unix, and Linux platforms in order to reach a great number of users.

4 Sensitivity Analysis

Because first principles calculations on fluorite, rocksalt, perovskite and pyrochlores materials performed by Aidhy and coworkers, show that charged oxygen vacancies contract the crystalline lattice [13], we tested several chemical expansion coefficients of $[\mathrm{V}_{\mathrm{O}}^{\cdot\cdot}]$, and $[\mathrm{Gd}_{\mathrm{Ce}}^{\prime}]$ by setting the experimentally measured total chemical expansion, $\beta_T = \beta^{(O)} + \beta^{(Gd)}$, as a constant, while $\beta^{(O)} \leq 0$. Values representative of the sensitivity analysis for $\mathrm{Gd}_y\mathrm{Ce}_{1-y}\mathrm{O}_{2-y/2}$, $y = 0.01$, are shown in Figure 1. Results herein demonstrate that for $\beta^{(O)} < 0$, and $\beta^{(Gd)} > \beta_T$, the stresses at the interface are unphysically high. In addition, negative values of $\beta^{(O)}$ induces an unphysical amount of oxygen vacancies at the grain boundary core. Further, negative values of $\beta^{(O)}$ and $\beta^{(Gd)} > \beta_T$ suppress the $[\mathrm{Gd}'_{\mathrm{Ce}}]$ content at the grain boundary, which contradicts experimental evidence of $[\mathrm{Gd}'_{\mathrm{Ce}}]$ accumulation at the grain boundary [10]. Finally, the excess accumulation of $[\mathrm{V}_{\mathrm{O}}^{\cdot\cdot}]$ make the ionic conductivity unphysically low.

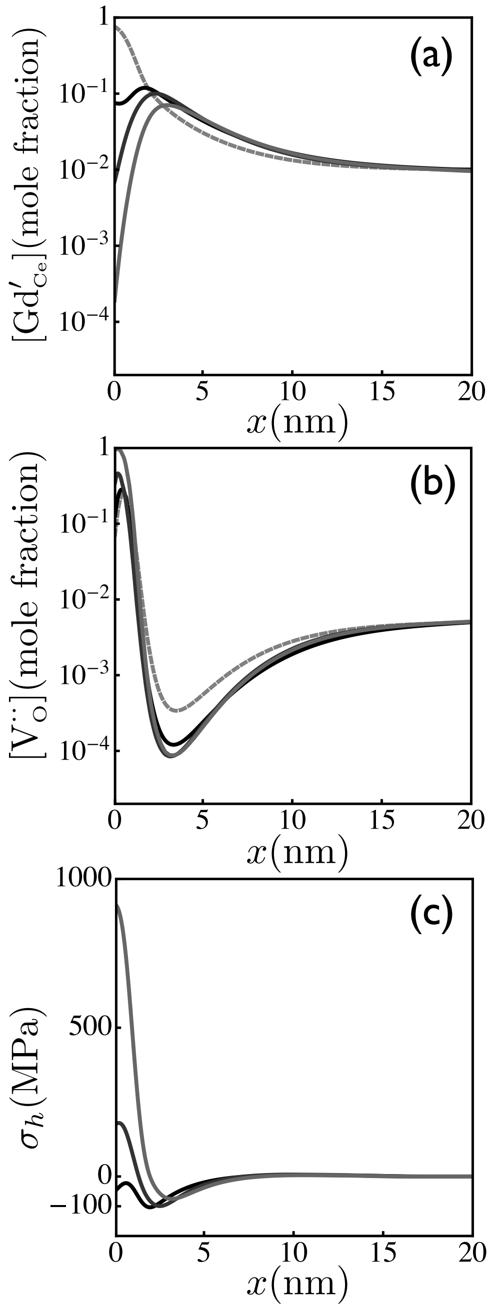

Figure 1: Effect of different contributions of Vegard expansion constant for $[\mathrm{V}_{\mathrm{O}}^{\cdot\cdot}]$ and $[\mathrm{Gd}'_{\mathrm{Ce}}]$ in $\mathrm{Gd}_y\mathrm{Ce}_{1-y}\mathrm{O}_{2-y/2}$, for $y = 0.01$, for a fixed total chemical expansion, $\beta_T = \beta^{(O)} + \beta^{(Gd)}$. Inset (a) shows predicted $[\mathrm{Gd}'_{\mathrm{Ce}}]$ spatial distribution, inset (b) shows predicted $[\mathrm{V}_{\mathrm{O}}^{\cdot\cdot}]$ spatial distribution, and inset (c) shows hydrostatic stress distribution. The black line corresponds to, $\beta^{(O)} = 0.0$, $\beta^{(Gd)} = 0.00095$, light gray line corresponds to $\beta^{(O)} = -0.000475$, $\beta^{(Gd)} = 0.001425$, and dark gray line corresponds to $\beta^{(O)} = -0.00095$, $\beta^{(Gd)} = 0.0019$. As a reference, the dash gray line shows predicted defect distribution in the absence of any mechanical and chemomechanical couplings.

References

[1] R. Kobayashi, J. A. Warren, W. C. Carter. "A Continuum Model of Grain Boundaries." *Physica D,* 140, 141–150, (2000).

[2] J. A. Warren, R. Kobayashi, A. E. Lobkovsky, W. C. Carter. "Extending Phase Field Models of Solidification to Polycrystalline Materials." *Acta. Mater.,* 51, 6035–6058, (2003).

[3] M. Tang, W. C. Carter, R. M. Cannon. "Grain Boundary Transitions in Binary Alloys." *Phys. Rev. Lett.,* 97, 075502, (2006).

[4] S. Zha, C. Xia, G. Meng. "Effect of Gd(Sm) Doping on Properties of Ceria Electrolyte For Solid Oxide Fuel." *J. Power Sources,* 115, 44–48, (2003).

[5] J. E. Guyer, D. Wheeler, J. A. Warren. "FiPy: Partial Differential Equations with Python." *Comput. Sci. Eng.,* 11, 615, (2009).

[6] A. C. E. Reid, R. C. Lua, R. E. García, V. R. Coffman, S. A. Langer. "Modelling Microstructures with OOF2." *Int. J. Mat. and Prod. Tech.,* 35, 361373, (2009).

[7] X. Guo. "Physical Origin of the Intrinsic Grain-Boundary Resistivity of Stabilized-Zirconia: Role of the Space-Charge Layers." *Solid State Ionics,* 81, 235-242, (1995).

[8] R. A. McKee. "A Generalization of the Nernst-Einstein Equation for Self-Diffusion in High Defect Concentration Solids." *Solid State Ionics,* 5, 133-136, (1981).

[9] X. Guo, R. Waser. "Electrical Properties of the Grain Boundaries of Oxygen Ion Conductors: Acceptor-Doped Zirconia and Ceria." *Prog. in Mat. Sci.,* 51, 151-210, (2006).

[10] A. Tschöpe, S. Kilassonia, R. Birringer. "The Grain Boundary Effect in Heavily Doped Cerium Oxide." *Solid State Ionics,* 173, 57–61, (2004).

[11] S. Grieshammer, B. O. H. Grope, J. Koettgen, M. Martin. “A Combined DFT+U and Monte Carlo Study on Rare Earth Doped Ceria.” *Phys. Chem. Chem. Phys.,* 16, 9974–9986, (2014).

[12] R. Pornprasertsuk, P. Ramanarayanan, C. B. Musgrave, F. B. Prinz. “Predicting Ionic Conductivity of Solid Oxide Fuel Cell Electrolyte from First Principles.” *J. Appl. Phys.,* 98, 103513, (2005).

[13] D. S. Aidhy, B. Liu, Y. Zhang, W. J. Weber. “Chemical Expansion Affected Oxygen Vacancy Stability in Different Oxide Structures from First Principles Calculations.” *Comp. Mat. Sci.,* 99, 298-305, (2015).